Environmental forcing on northeast Atlantic bluefin tuna abundance

Ricardo T. Lemos*, Bruno Sansó † and Henrique N. Cabral ‡

Abstract

In this work we present a framework that blends time series and geostatistical methods to analyze the association between northeast Atlantic bluefin tuna abundance, August sea surface temperature, zonal wind speed and the North Atlantic Oscillation, during the 19th and 20th centuries. We describe how to extract a dominant nonlinear trend in each data type, check parameter convergence and assess goodness-of-fit. Temporal autocorrelation and spatial residual coherence are accounted for, even in data sets with abundant missing values. We also provide a means to do regression analysis that propagates estimation uncertainty. Such an approach brings novel methods to the field of ecological analysis. Results show that bluefin tuna abundance fluctuated widely in the last 200 years, with a possible link to the predictor variables selected. A causal chain is discussed, followed by a reflection on the current status of the stock.

1 Introduction

In several regions of the Mediterranean and adjacent Atlantic, fisheries for northern bluefin tuna, *Thunnus thynnus* (L.), have for long been prosperous activities, some since prehistorical times (Doumenge, 1998). Their social and economic importance is testified by the direct management of some by monarchs and nobles, the development of coastal settlements around them, and the depiction of tuna in coins (Galvão, 1953). Due to the high market value of bluefin meat, this population is at present heavily overfished, with international recovery measures facing difficulties (Fromentin and Powers, 2005).

Traditional fishing devices for bluefin may be classified into five different types: harpoons, hooks, trammel nets, seines and traps (Mather et al., 1995). Until the recent (<60yr) development of purse seining, live bait and longlining, traps were the gear responsible for most catches (Doumenge, 1998). In short, a trap is a set of barriers and chambers, made of net, which extend from the shallow sea floor to the surface. As they approach the coast, migrating tuna schools are led by the barriers into the chambers, where they are gaffed.

*NOAA/NMFS Environmental Research Division Southwest Fisheries Science Center 1352 Lighthouse Avenue Pacific Grove, CA 93950-2097 USA. E-mail ricardo.delemos@noaa.gov

†Department of Applied Mathematics and Statistics, University of California, 1156 High St. MS:SOE2, Santa Cruz, CA-95064, U.S.A. E-mail bruno@ams.ucsc.edu, www.ams.ucsc.edu/∼bruno

‡Centro de Oceanografia, Universidade de Lisboa, Campo Grande, 1749-016 Lisboa, Portugal.

Thanks to careful bookkeeping, records of numerous traps' annual yields are available in the scientific literature, some extending over centuries. The depiction of these time series reveals ample temporal variability, with two characteristic patterns. The first corresponds to year-to-year variability, up to sub-decadal cycles. These are site-specific and have been attributed to local oceanographic conditions; for example, when coastal waters are turbid, tuna schools tend to migrate farther offshore, thereby reducing traps' yields (Lemos and Gomes, 2004). In other words, this high frequency variability reflects changes in bluefin's spatial distribution, not abundance. The second, more prominent pattern of variability comprises long-term fluctuations, which seem synchronous across the coasts of Portugal, Spain, Morocco, Italy, Sicily, Sardinia and Tunisia (Ravier and Fromentin, 2001, and references therein). As the exchange of correspondence between the Duque of Medina Sidonia and Fray Martín Sarmiento demonstrates (1757; in de Buen, 1925), trap owners and scholars have wondered about the nature of these fluctuations for a long time. One possible explanation is that: i) they correspond to actual changes in bluefin tuna abundance; and ii) these changes occur in response to some natural forcing.

Let us substantiate the first claim, by briefly reviewing its merits and some demerits of alternative hypotheses. According to Ravier and Fromentin (2001), long-term fluctuations in trap catches are unlikely to result from social and economic factors, given the multitude of countries where they are observed; nor do they correspond to "boom and bust" fishery cycles, since prior to World War II (WWII), fishing effort was relatively low and stable. Shifts in bluefin distribution are also improbable, since the above mentioned network of traps encircles most of bluefin's distribution range in the Mediterranean and adjacent NE Atlantic, during the spawning season. These traps are passive gears, whose location and operation remained nearly constant for centuries. A few technological developments slightly improved their efficiency over the years, but at the same time, increasing coastal traffic and pollution progressively reduced it (Sarà, 1980). Therefore, they may be regarded as samplers that capture the same proportion of the migrating bluefin tuna population each year (Ravier and Fromentin, 2001), once we filter out the confounding sub-decadal sources of variability.

With respect to the second claim, various researchers have found connections between bluefin abundance and environmental factors (Borja and Santiago, 2002; Ravier and Fromentin, 2004; Bridges et al., 2009; Ganzedo et al., 2009), but results are not conclusive. Searching a different path, Fromentin (2002) used simulated data to show that long-term pseudo-cycles in bluefin abundance can be caused by a noisy, but cycle-free environment. This occurs because, in the case of a long lived species such as bluefin tuna, the spawning stock includes several cohorts, thus smoothing high frequency recruitment variability into a lower frequency signal. However, the same author notes that this does not rule out the claim that tuna abundance may be driven by climatic cycles, and concludes that the latter remain elusive.

The goal of the present paper is to contribute to this search. If a natural cause for long-term cycles exists, it should act on a large spatial scale, such as bluefin's spawning and feeding grounds. The Mediterranean Sea emerges as the most interesting region, since adults converge to it to breed, and young tuna use it throughout the year. With respect to time, we focus on August. During this month, the annual reproduction period is culminating, and the life stages (eggs, larvae and early juveniles) most vulnerable to climatic fluctuations

are abundant (Borja and Santiago, 2002). Simultaneously, post-spawners are seeking food to replenish themselves (Sarà, 1963). Therefore, mechanisms associated with enrichment, concentration and retention can be sought as causes for the cycles in bluefin tuna abundance.

Although weaker than its winter counterpart, the summer North Atlantic Oscillation (NAO) has been shown to exert a significant influence on European climate, including cloudiness, rainfall and surface temperature (Folland et al., 2009). Hence, a NAO index would be an interesting candidate predictor. Likewise, indexes that summarize sea surface temperature (SST) and zonal air flow over the Mediterranean, may provide complementary information and be interpretable from an ecological standpoint (see e.g. Sarà, 1963; Rodewald, 1967; Binet and Leroy, 1987, on how wind and SST may be linked to tuna distribution).

In this work, we use a hierarchical Bayesian model to perform several tasks. The first is to construct synthetic time series of tuna abundance and environmental indexes, which account for spatial and temporal structures, as well as measurement error; the weighting scheme used to construct these indexes is part of the estimation procedure. The second task is to obtain transient trends in the indexes, using a polynomial trend model (West and Harrison, 1997). The third task is to assess if the bluefin abundance trend is linked to one or several environmental trends, given the levels of uncertainty determined by the data and the model construction. Thus, in a single, hierarchical framework, we are combining several methods used in previous research. The disparity between data sets (gridded vs. non-gridded data, sparse vs. complete records, high vs. low signal-to-noise ratio, short vs. long term memory) shows the flexibility of the approach, which can be generalized for other ecological analyses.

2 Data and Model

Two August NAO proxies, which we denote as $Y_t^{\text{NAO}}(k)$, can be retrieved from the Climatic Research Unit's data library (`http://www.cru.uea.ac.uk`). They consist of normalized pressure differences between Reykjavik and either Gibraltar ($k = 1$) or Ponta Delgada ($k = 2$); $t = 1821, \ldots, 2000$ indicates the year. Gridded August means of geostrophic zonal wind speed over the Mediterranean and adjacent Atlantic ($Y_t^{\text{u-wind}}(k)$, where $k = 1, \ldots 44$ denotes the grid point) derive from HadSLP2 (`http://www.hadobs.org/`), a 5° monthly mean sea level pressure data set spanning from 1850 to 2000. Mediterranean 2° gridded August sea surface temperature anomalies ($Y_t^{\text{SST}}(k), k = 1, \ldots 84$) range between 1854 and 2000. The data set (Smith et al., 2008) is available at the International Research Institute for Climate and Society and the Lamont-Doherty Earth Observatory (`http://iridl.ldeo.columbia.edu`). Finally, we use 54 time series of Atlantic and Mediterranean trap catches, in number of bluefin tuna caught per year ($C_t(k)$; Table 1). We log-transform these data, yielding $Y_t^{\text{BFT}}(k)$.

In the following expressions, the superscript i denotes any of the four data types: NAO, u-wind, SST and BFT. The model is:

$$Y_t^i(k) = \theta^i(k) + \omega^i(k)\mu_t^i + \epsilon_t^i(k) \tag{1}$$

$$\epsilon_t^i(k) \sim N\left(0, \tau^i\right), \mathrm{Cov}(\epsilon_t^i(k), \epsilon_t^i(k')) = \tau^i(1 + d_{k,k'}^i/\phi^i)\exp(-d_{k,k'}^i/\phi^i) \tag{2}$$

$$\mu_t^i = \mu_{t-1}^i + \alpha_t^i, \tag{3}$$

$$\alpha_t^i = \rho^i \alpha_{t-1}^i + \xi_t^i \tag{4}$$

$$\xi_t^i \overset{\text{ind.}}{\sim} \mathrm{N}(0, \sigma^i), \tag{5}$$

where $\mu_t^i \in \mathbb{R}$ is the underlying atmospheric, oceanic or log-abundance index, N denotes the Normal distribution, $\tau^i, \sigma^i \in \mathbb{R}_0^+$ are variance parameters, $\phi^i \in \mathbb{R}_0^+$ is the covariance decay parameter, $\omega^i(k) \in \mathbb{R}$ is the weight assigned to the k-th time series of data type i, $\alpha_t^i \in \mathbb{R}$ is an annual nonlinear trend and $\rho^i \in (-1, 1)$ is an autocorrelation parameter. In equation (2), the Matérn covariance function, with smoothness parameter equal to 1.5, is used to account for residual spatial covariance (Banerjee et al., 2004). The distance between points k and k' of data set i, $d_{k,k'}^i$, is approximated by the haversine formula (Sinnott, 1984). For NAO, we set $d_{k,k'}^i = 100$km. We fix $\omega^i(1) = 1$, for all i, and use the following priors: $\tau^i, \sigma^i \overset{\text{iid}}{\sim} \mathrm{Exp}(10^{-5})$, $\phi^i \overset{\text{iid}}{\sim} \mathrm{U}(0, 10^6)$, $\theta^i(k) \overset{\text{iid}}{\sim} \mathrm{N}(0, 10)$, $\beta^{i'} \overset{\text{iid}}{\sim} \mathrm{N}(0, 10^5)$, $\rho^i \overset{\text{iid}}{\sim} \mathrm{U}(-1, 1)$, and $\omega^i(k) \overset{\text{iid}}{\sim} \mathrm{N}(1, 0.1)$ if $k > 1$. $\mathrm{Exp}(r)$ and $\mathrm{U}(l, u)$ stand for the Exponential and Uniform distributions, with rate r and support (l, u).

The model for the environmental variables can be interpreted as follows: consider that the various records of SST, u-wind, and standardized air pressure differences share a common, non-stationary pattern of temporal variability, respectively μ_t^{SST}, $\mu_t^{\text{u-wind}}$ and μ_t^{NAO}. Each pattern is governed by a trend, α_t^i, which evolves as an autoregressive process of order one (AR-1). The quantity $\omega^i(k)$ is a weight associated with that pattern, $\theta(k)$ is the long-term mean, and the Matérn covariance function accounts for the remaining spatial structure.

The biological model requires additional formulas to be understood. Let N_t denote the abundance of NE Atlantic bluefin tuna in year t. We describe the temporal evolution of abundance with the equation $N_t = N_{t-1}e^{\alpha_t}$ or, equivalently, $N_t = N_0 e^{\mu_t}$, where μ_t accumulates the annual rates of population change: $\mu_t = \sum_{j=0}^{t} \alpha_j$. Note that e^{μ_t} provides the rate between abundances at times t and 0, and $\alpha_0 = 0$. For $t > 0$, we assume that α_t^{BFT} follows an AR-1. Bluefin tuna abundance is not observed directly; only catches data are available, from a number of traps. We assume a flexible relationship between the two: $N_t = f_t(k)(C_t(k))^{p(k)}$, where the power and the time-varying proportionality coefficient are respectively given by $p(k) = 1/\omega^{\text{BFT}}(k)$ and $f_t(k) = N_0 \exp[-(\theta^{\text{BFT}}(k) + \epsilon_t^{\text{BFT}}(k))/\omega^{\text{BFT}}(k)]$. Note that N_0 is inserted here for convenience and cannot be estimated (nor can any other N_t). It is sensible to expect that the transient fluctuations of f_t are coherent across space, and for that reason we model $\mathrm{Cov}(\epsilon_t^{\text{BFT}}(k), \epsilon_t^{\text{BFT}}(k'))$ with the Matérn covariance function. By combining the expressions above and taking logarithms, we obtain the biological model.

Equations 1-5 correspond to a Dynamic Linear Model (West and Harrison, 1997), if white Gaussian noise with negligible variance is added to the right-hand side of equation 3. To explore the posterior distribution of the parameters, we employ Markov chain Monte Carlo methods (MCMC; Gelman et al., 2004; Gamerman and Lopes, 2006): we use Gibbs steps

Table 1: **Trap catches metadata** - names, approximate coordinates, first and last years with data, number of years with data, and data sources: (1) Rodríguez-Roda (1983); (2) Garcia et al. (2002); (3) Piccinetti and Omiccioli (1999); (4) Heldt (1932); (5) Anonymous (1974).

Name, country	Location	Data(N)	Ref.	Name, country	Location	Data(N)	Ref.
Barbate, ES	36.17° N,6.04° W	1910-1982(65)	1	Zliten, LY	32.47° N,14.57° E	1925-1934(10)	4
Lances de Tarifa, ES	35.99° N,5.61° W	1914-1982(50)	1	Marsa Sabrata, LY	32.81° N,12.49° E	1921-1931(10)	4
Punta de la Isla, ES	36.39° N,6.24° W	1917-1971(50)	1	Sidi Abd El Gelil, LY	32.84° N,13.02° E	1920-1930(10)	4
Nueva Umbria, ES	37.05° N,6.70° W	1916-1965(42)	1	Ras Lahmar, LY	32.88° N,13.14° E	1920-1929(10)	4
Zahara, ES	36.13° N,5.87° W	1910-1982(27)	1	Medo das Cascas, PT	37.10° N,7.60° W	1852-1969(118)	5
Las Torres, ES	37.05° N,6.72° W	1902-1933(22)	1	Senhora do Livramento, PT	37.04° N,7.73° W	1896-1969(74)	5
Arroyo Hondo, ES	36.64° N,6.43° W	1914-1933(18)	1	Barril, PT	37.06° N,7.67° W	1896-1966(71)	5
Reina Regente, ES	37.15° N,7.37° W	1914-1933(18)	1	Abóbora, PT	37.15° N,7.53° W	1896-1965(70)	5
Torre Atalaia, ES	36.26° N,6.13° W	1914-1931(17)	1	Cabo de Santa Maria	36.96° N,7.96° W	1898-1967(57)	5
La Higuera, ES	36.87° N,6.46° W	1914-1928(14)	1	Ramalhete, PT	37.01° N,8.02° W	1896-1937(42)	5
Nuestra Sra. Cinta, ES	37.15° N,6.95° W	1914-1928(13)	1	Lagos, PT	37.08° N,8.66° W	1809-1845(36)	5
Las Cabezas, ES	37.15° N,7.35° W	1914-1928(10)	1	Sul da Ponta do Baleal, PT	36.99° N,8.93° W	1902-1926(25)	5
Portoscuso, IT	39.60° N,8.40° E	1825-2000(168)	2	Olhos de Água, PT	37.06° N,8.22° W	1896-1919(24)	5
Isola Piana, IT	39.20° N,8.22° E	1825-2000(164)	2	Senhora da Rocha, PT	37.09° N,8.37° W	1897-1920(24)	5
Favignana, IT	37.97° N,12.30° E	1810-1979(69)	3	Forte Novo	37.06° N,8.15° W	1896-1918(23)	5
Carloforte, IT	39.14° N,8.31° E	1868-1995(67)	3	Torre da Barra, PT	37.09° N,8.51° W	1897-1917(21)	5
Saline, IT	40.96° N,8.27° E	1868-1930(63)	3	Sul do Cabo Carvoeiro, PT	37.07° N,8.44° W	1896-1917(21)	5
Tono, IT	38.31° N,15.22° E	1896-1931(50)	3	Medo Branco, PT	37.06° N,8.24° W	1896-1915(20)	5
Bonagia, IT	38.13° N,12.65° E	1809-2000(44)	3	Bias, PT	37.02° N,7.76° W	1896-1921(20)	5
Pizzo, IT	38.96° N,16.10° E	1876-1928(44)	3	Sul da Ponta do Zavial, PT	37.00° N,8.92° W	1897-1911(15)	5
Oliveri, IT	38.25° N,15.33° E	1904-1964(43)	3	Torre Altinha, PT	37.08° N,8.67° W	1896-1909(14)	5
San Cosumano, IT	38.00° N,12.47° E	1950-1964(15)	3	Sidi Daoud, TN	37.02° N,10.89° E	1863-1930(67)	3
San Giorgio, IT	38.29° N,15.22° E	1950-1963(14)	3	Conigliera, TN	35.76° N,11.02° E	1897-1929(32)	3
Magazzinazzi, IT	38.06° N,12.93° E	1950-1961(12)	3	Ras El Ahmar, TN	37.05° N,10.91° E	1905-1930(25)	3
San Giuliano, IT	38.02° N,12.52° E	1896-1911(11)	3	Monastir, TN	35.78° N,10.83° E	1894-1926(24)	3
Scopello, IT	38.08° N,12.84° E	1955-1964(10)	3	Borj Khadija, TN	35.23° N,11.15° E	1904-1929(21)	3
				El Aouaria, TN	37.05° N,11.01° E	1907-1930(17)	3
				Kuriat, TN	35.78° N,10.90° E	1904-1927(15)	3

to sample $\theta_t^i(k)$, $\beta^{i'}$ and $\omega^i(k)$, the Backward Sampling algorithm to sample μ_t^i and α_t^i, and we use Metropolis-Hastings (M-H) steps, with the Forward Filtering algorithm, to sample $\tau^i, \phi^i, \sigma^i, \rho^i$.

With the posterior samples from this model, we regress the log-abundance index to a linear combination of the environmental indexes:

$$\mu_t^{\text{BFT}} = \beta^{\text{BFT}} + \beta^{\text{NAO}}\mu_t^{\text{NAO}} + \beta^{\text{u-wind}}\mu_t^{\text{u-wind}} + \beta^{\text{SST}}\mu_t^{\text{SST}} + \upsilon_t, \tag{6}$$

$$\upsilon_t \overset{\text{iid}}{\sim} \text{N}(0,\tau), \quad p(\tau) \propto 1/\tau, \quad \beta^i \overset{\text{iid}}{\sim} \text{N}(0, 10^{20}\tau), \tag{7}$$

We also analyze the distribution of $R^i = \text{Corr}(\alpha_t^{\text{BFT}}, \alpha_t^i)$, i.e., the correlation that operates on the differenced indexes.

Hence, our strategy to characterize the posterior distribution of all parameters is as follows. Let $\boldsymbol{\lambda}^i$ denote the collection of the parameters in equations 1-5, and let $\boldsymbol{\Lambda} = \{\boldsymbol{\lambda}^{\text{NAO}}, \boldsymbol{\lambda}^{\text{u-wind}}, \boldsymbol{\lambda}^{\text{SST}}, \boldsymbol{\lambda}^{\text{BFT}}\}$. Analogously, $\boldsymbol{y}^i$ represents all the data from data type i, and $\boldsymbol{Y}$ is the full data set. Finally, let $\boldsymbol{\Omega}$ collect the parameters in expressions 6-7. Assuming that the estimation of $\boldsymbol{\lambda}^i$ depends solely on the corresponding data, $\boldsymbol{y}^i$, we obtain the factorization:

$$p(\boldsymbol{\Lambda}|\boldsymbol{Y}) = p(\boldsymbol{\lambda}^{\text{NAO}}|\boldsymbol{y}^{\text{NAO}}) \times p(\boldsymbol{\lambda}^{\text{u-wind}}|\boldsymbol{y}^{\text{u-wind}}) \times p(\boldsymbol{\lambda}^{\text{SST}}|\boldsymbol{y}^{\text{SST}}) \times p(\boldsymbol{\lambda}^{\text{BFT}}|\boldsymbol{y}^{\text{BFT}}). \tag{8}$$

Owing to this assumption, we fit an independent model for each data type. Then, we use that $p(\boldsymbol{\Omega}, \boldsymbol{\Lambda}|\boldsymbol{Y}) = p(\boldsymbol{\Omega}|\boldsymbol{\Lambda}, \boldsymbol{Y}) \times p(\boldsymbol{\Lambda}|\boldsymbol{Y})$, which stems from standard probability theory, to sample the regression parameters ($\boldsymbol{\Omega}$) using the posterior samples from the other parameters ($\boldsymbol{\Lambda}$).

3 Results

Results are based on 1,000 MCMC iterations, spaced 20 iterations apart, after a burn-in of 30,000 iterations, which includes a period of learning for M-H jumping kernels. Analysis of these samples indicates the chain converged for all parameters. Furthermore, visual inspection of qq-plots from the one-step ahead distributions, as well as time series plots of fitted versus observed values (e.g., Figure 1, left panels), leads us to assume the model fit is satisfactory. We refer the interested reader to the auxiliary material, for more details.

Temporal smoothness and uncertainty in the underlying indexes vary substantially among data types (Figure 1, central panels). The August NAO index presents the lowest signal-to-noise ratio, followed by the log-abundance index. In both, long term fluctuations predominate. In contrast, u-wind and SST indexes have narrow 95% credibility intervals, and their mean contains transient variability. In agreement with this, the nonlinear annual trends for u-wind and SST often digress from zero, while the opposite is true for the NAO and log-abundance trends (Figure 1, right panels).

Although spatial coherence was not provided in the prior distribution of the weights associated with the u-wind index, a clear pattern emerges in the posterior means (Figure 2, upper panel): from 45°N, 10°W, where the largest value is found, weights gradually decay, more rapidly with latitude than with longitude. The posterior mean of SST weights is also spatially smooth (Figure 2, central panel). Weights are larger in the Adriatic Sea and

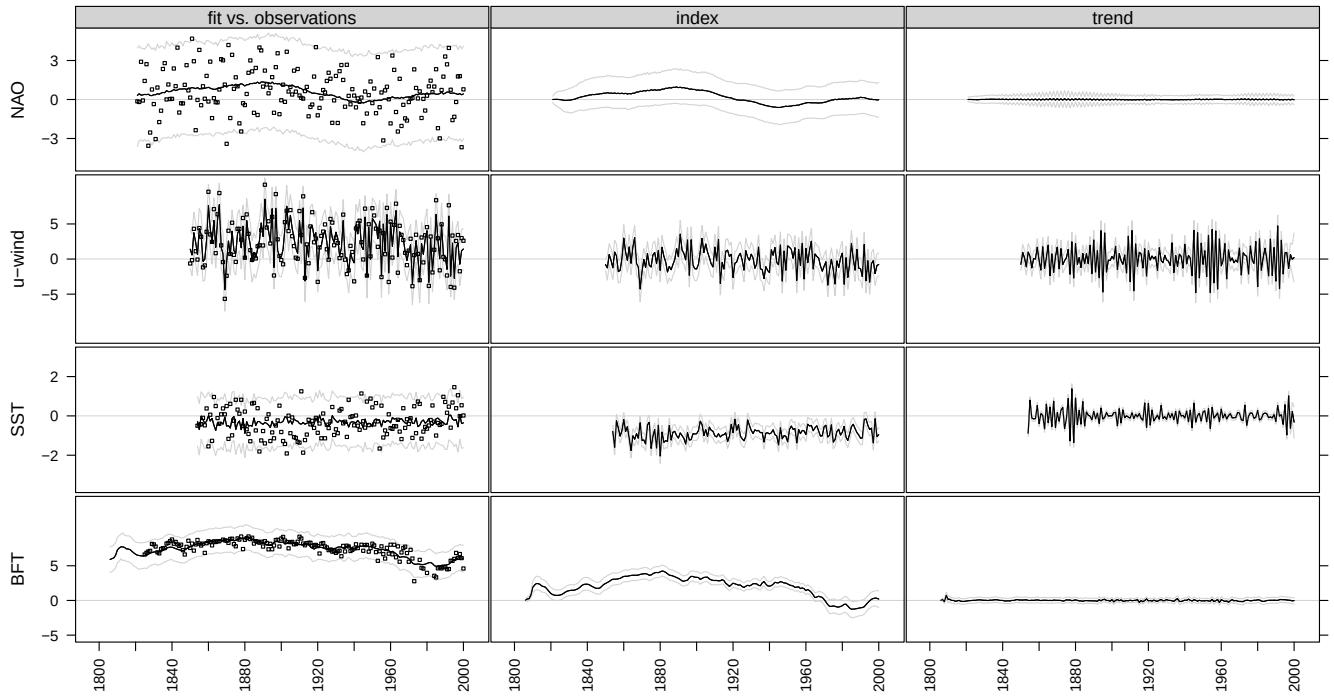

Figure 1: Model fit, indexes and trends. Left hand panels: observations (squares) and fitted values (black and gray lines denote posterior means and 95% credibility intervals, respectively) for the Gibraltar-Reykjavik NAO proxy, u-wind at 45°N, 5°W, SST at 46°N, 30°E, and log trap catches at Favignana. Central panels: posterior distribution of the environmental and log-abundance indexes (μ_t^i). Right-hand panels: posterior distribution of the annual trends (α_t^i).

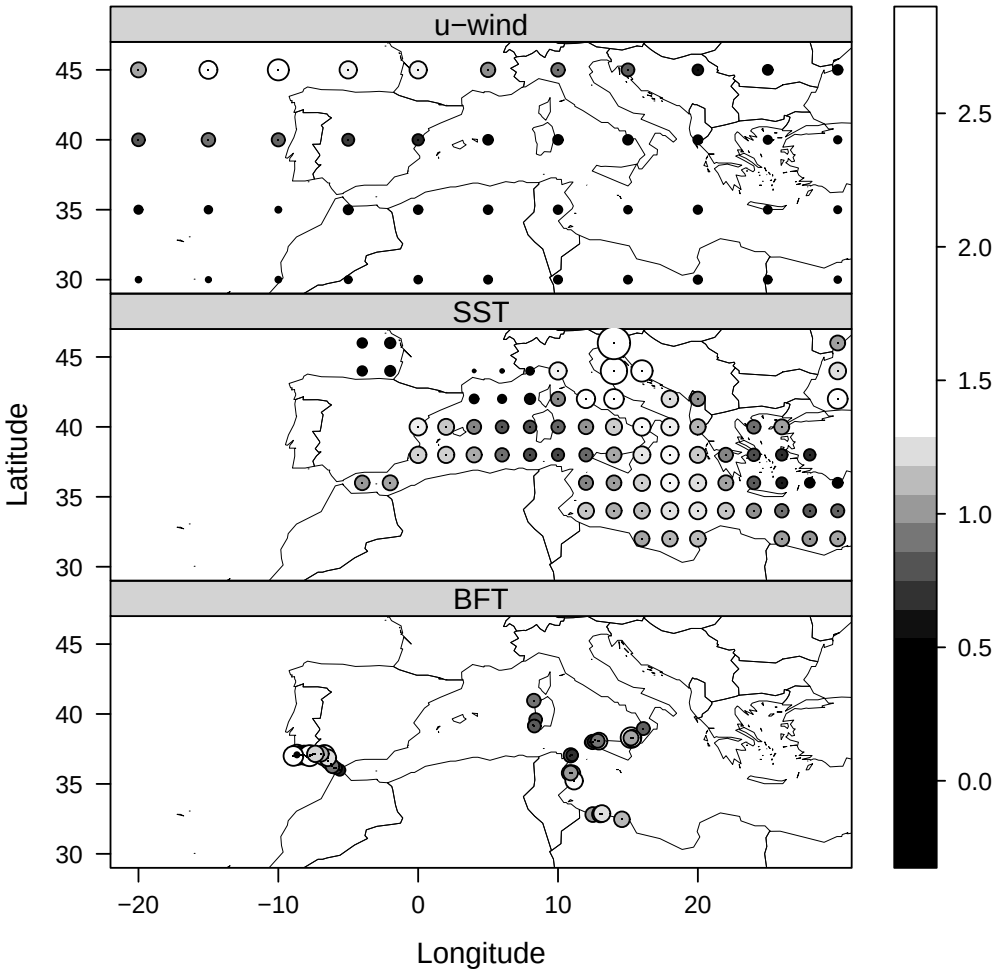

Figure 2: Spatial distribution of the posterior mean of the weights $\omega^i(k)$ (see eq. 1). The circle size is proportional to the mean. Black dots denote grid points and traps.

remain close to 1 in much of the Mediterranean, with the exception of the Gulf of Lion and the Aegean Sea. Subtler patterns in traps weights can also be found (Figure 2, lower panel): from SW Portugal to the Gibraltar Strait, trap weights tend to decrease; in the Mediterranean, small weights concentrate in the triangle that connects Sardinia, Sicily and Libya. As a result, long-term fluctuations in catches are less evident in the mouth and central parts of the Mediterranean than elsewhere (cf. the Favignana fit vs. the index, in Figure 1).

Once the mean and the dominating index have been accounted for in the observations, the amount of residual spatial structure differs among data types: from the posterior means of ϕ^i (Table 2), we deduce that the decorrelation scale (i.e., the mean distance at which the correlation between $\varepsilon_t^i(k)$ and $\varepsilon_t^i(k')$ drops below 0.1) is: 1440km for u-wind residuals, 2840km for SST residuals, and 4.6km for log-catches. Given the grid resolutions considered, assumptions of spatial independence for u-wind and SST residuals would thus be untenable.

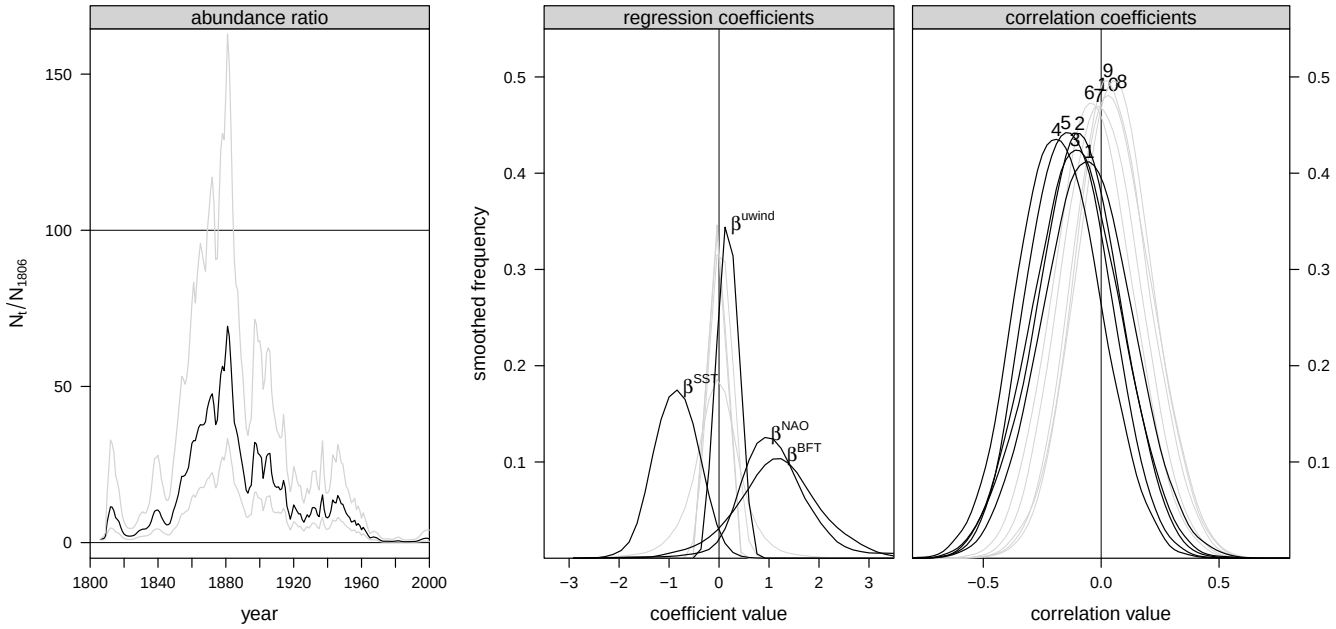

Figure 3: Evolution of bluefin tuna relative abundance and the decay of environmental coupling. Left panel: posterior mean and 95% credibility intervals for $\exp(\mu_t^{\mathrm{BFT}})$, which equates to N_t/N_{1806}. Central panel: posterior distribution of the regression coefficients in model 6-7, for the full time span (black lines) and the post-WWII period (gray lines). Right panel: distribution of R^{SST} for overlapping periods of 60 years, starting at 1856-1915 (labeled 1) and ending at 1946-1995 (labeled 10), with 10 year shifts. Correlations that use post-WWII data are depicted in light gray.

Residuals from the two NAO proxies also present common structure; the posterior mean correlation is 0.7.

Index signal-to-noise ratios may be computed from σ^i/τ^i (Table 2). As mentioned before, the NAO index has the lowest value, meaning that the model, as we specified it, is not able to extract much structure from the data. Accordingly, the autocorrelation coefficient for the NAO index is the one with largest posterior uncertainty (Table 2).

With the results from this model, we may construct a probabilistic hindcast for the evolution of bluefin tuna abundance, relative to the abundance in the first year considered, 1806 (Figure 3). Uncertainty changes over time, being higher during peak abundance – a reflex of modeling log-catches with additive normal errors. Still, there are two noticeable features in this reconstruction: i) pre-WWII abundance levels were never stable, for long time periods; ii) abundance in the late 20th century is similar in value to that in the early 1800s, but dissimilar in variability – it remains low for almost 30 years.

Bearing this in mind, we run the regression model with the complete indexes first, and then we use only post-WWII data. The difference is striking (Figure 3, central panel): with the full time span, the posterior distributions of β^{NAO} and $\beta^{\text{u-wind}}$ are mainly positive, while that of β^{SST} is mainly negative. In contrast, post-WWII distributions are centered at zero, indicating no correlation between environmental variability and abundance. Although

Table 2: Posterior means and 95% credibility intervals for some model parameters. The posterior probability that each β coefficient is negative appears in square brackets.

	NAO	u-wind	SST	BFT
ϕ^i	$9.1 \times 10^4 (7.1 \times 10^4, 1.1 \times 10^5)$	$3.7 \times 10^5 (3.6 \times 10^5, 3.9 \times 10^5)$	$7.3 \times 10^5 (7.0 \times 10^5, 7.6 \times 10^5)$	$1.2 \times 10^3 (2.8 \times 10^2, 2.5 \times 10^3)$
σ^i	$0.0077(0.0005, 0.0272)$	$1.31(0.82, 1.93)$	$0.065(0.047, 0.090)$	$0.039(0.019, 0.066)$
τ^i	$3.2(2.7, 3.9)$	$1.5(1.4, 1.6)$	$0.40(0.37, 0.45)$	$0.79(0.57, 1.08)$
ρ^i	$-0.33(-0.98, 0.70)$	$-0.86(-0.94, -0.78)$	$-0.83(-0.92, -0.75)$	$-0.30(-0.68, 0.28)$
β^i	$1.20(-0.98, 3.26)[0.036]$	$0.179(0.015, 0.363)[0.015]$	$-0.83(-1.634, -0.05)[0.987]$	$1.20(-0.34, 3.00)[0.078]$

the bluefin index trend remains close to zero and contains much imprecision (Figure 1), it appears to be negatively correlated with SST until WWII (Figure 3, right panel). From then onwards, the correlation weakens and changes sign.

4 Discussion

Time series of trap catches are highly fragmentary, which renders the construction of a composite abundance index difficult. Here we show one way to construct such an index. Given the posterior distribution of the weights and the weak residual correlation, we conclude that the index captures the bulk of variability in the 54 time series, and argue that it is an adequate long-term surrogate for Northeast Atlantic bluefin tuna abundance. If we assume that fisheries did not have a significant impact before the mid 20th century, it logically follows that the carrying capacity for this population is highly variable, since abundance may have fluctuated by two orders of magnitude (Figure 3). Therefore, a pristine-state, stable reference level may not exist for this stock.

From the weights (Figure 2), we observe that in times of tuna scarcity, traps located in the central Mediterranean and near the Strait of Gibraltar are less impacted than those in the periphery. This means not all regions visited by tuna schools during the reproductive period reflect abundance fluctuations with the same intensity. It may explain, for example, why Portuguese traps ceased activity mostly in the decades of 1910 and 1960, while some Spanish traps were able to keep operating until the end of the century.

The immediate issue is the origin of abundance fluctuations. Our regression analysis suggests that the BFT index might, to some extent, be predicted by the NAO, u-wind and SST indexes. We also describe a coherent, weak negative correlation between the differenced indexes of BFT and SST (Figure 3). The high proportion of unexplained variance is expectable, given the nature of the variables being related (Figure 1). Bluefin abundance estimates change slowly over time and present large uncertainty, as they are constructed from noisy fisheries data. SST and u-wind indexes, on the other hand, have substantial interannual variability, due to the shorter memory of oceanic and atmospheric processes. The August NAO index appears difficult to differentiate from white noise. Hence, the regression analysis we have presented serves only to detect a possible association, and should be followed by models with added complexity.

As mentioned above, the connections between indexes and trends disappear after the mid 20th century. This may be because pre-WWII correlations were spurious, but we suspect fishing pressure causes the apparent decoupling. Unlike any other period, post-WWII abundance remains stable and low, roughly reaching 35% of 1806 values in 1985. Thus, in the same manner that fishing impacts are confounded by climate variability, the converse is also true. We conclude that an integrated model of fisheries and environmental drivers is the most promising tool to understand the nature of bluefin's abundance variability.

5 Acknowledgments

The first author acknowledges grant SFRH/BD/17929/2004 from Fundação para a Ciência e a Tecnologia, used in the preparation of an earlier manuscript. The second authors was partially supported by the National Science Foundation Grant DMS-0906765.

References

Anonymous (1974). Estatísticas das Pescas no Continente e Ilhas Adjacentes. Technical report, Lisboa: Imprensa da Armada.

Banerjee, S., Carlin, B., and Gelfand, A. (2004). *Hierarchical Modeling and Analysis of Spatial Data*. Chapman and Hall, New York.

Binet, D. and Leroy, C. (1987). La pêcherie du thon rouge (Thunnus thynnus) dans l'Atlantique Nord est-elle liée au réchauffement séculaire? *Collective Volume of Scientific Papers ICCAT*, 26:314–322.

Borja, A. and Santiago, J. (2002). Does the North Atlantic Oscillation control some processes influencing recruitment of temperate tunas? *Collective Volume of Scientific Papers ICCAT*, 54(4):964–984.

Bridges, C., Krohn, O., Deflorio, M., and de Metrio, G. (2009). Possible NAO and SST influences on the Eastern bluefin tuna stock - the IN-EXFISH approach. *Collective Volume of Scientific Papers ICCAT*, 63:138–152.

de Buen, F. (1925). Biologia del atún (Orcynus thynnus L.). *Resultados de las campañas realizadas por acuerdos internacionales, Comm. Int. Mer Médit.*, 1:1–118.

Doumenge, F. (1998). L'histoire des pêches thonières. *Collective Volume of Scientific Papers ICCAT*, 50(2):753–803.

Folland, C., Knight, J., Linderholm, H., Fereday, D., Ineson, S., and Hurrell, J. (2009). The Summer North Atlantic Oscillation: past, present and future. *Journal of Climate*, 22(5):1082–1103.

Fromentin, J.-M. (2002). Can stochastic variations in recruitment induce long-term fluctuations in the carrying capacity? *Collective Volume of Scientific Papers ICCAT*, 54(4):985–991.

Fromentin, J.-M. and Powers, J. (2005). Atlantic bluefin tuna: population dynamics, ecology, fisheries and management. *Fish and Fisheries*, 6(4):281–306.

Galvão, A. (1953). *Um século de história da Companhia de Pescarias do Algarve*. Companhia de Pescarias do Algarve, Faro, 2nd edition.

Gamerman, D. and Lopes, H. F. (2006). *Markov Chain Monte Carlo - Stochastic Simulation for Bayesian Inference*. Chapman and Hall, London, UK, second edition.

Ganzedo, U., Zorita, E., Solari, A. P., Chust, G., Santana del Pino, A., Polanco, J., and Castro, J. J. (2009). What drove tuna catches between 1525 and 1756 in southern Europe? *ICES Journal of Marine Science*, 66(7):1595–1604.

Garcia, S., Dean, J., Addis, P., Fletcher, M., and Almeida, J. (2002). Identification of a predictive dynamical model for the Mediterranean tuna. In *International Conference on Mathematics and Biology and Annual Meeting of The Society for Mathematical Biology, Knoxville TN*.

Gelman, A., Carlin, J. B., Stern, H. S., and Rubin, D. B. (2004). *Bayesian Data Analysis, Second Edition*. Chapman & Hall/CRC.

Heldt, H. (1932). Le thon rouge et sa pêche (7ème rapport). *Rapport et Procès-verbaux des Réunions du Conseil International pour la Exploration de la Mer*, 7:203–318.

Lemos, R. and Gomes, J. (2004). Do local environmental factors induce daily and yearly variability in bluefin tuna (*Thunnus thynnus*) trap catches? *Ecological Modelling*, 177:143–156.

Mather, F., Mason Jr, J., and Jones, A. (1995). *Historical document: life history and fisheries of Atlantic bluefin tuna*. NOAA Technical Memorandum NMFS-SEFSC-370, Miami.

Piccinetti, C. and Omiccioli, H. (1999). Contribution à la connaissance des captures du thon rouge par les madragues. *Collective Volume of Scientific Papers ICCAT*, 49(2):444–455.

Ravier, C. and Fromentin, J.-M. (2001). Long-term fluctuations in the Eastern Atlantic and Mediterranean bluefin tuna population. *ICES Journal of Marince Science*, 58:1299–1317.

Ravier, C. and Fromentin, J.-M. (2004). Are the long-term fluctuations in Atlantic bluefin tuna (*Thunnus thynnus*) population related to environmental changes? *Fisheries Oceanography*, 13:145–160.

Rodewald, M. (1967). Transatlantic migrations of the bluefin tuna and the anomalies of the atmospheric circulation. *ICES CM (Pelagic Fish Committee)*, J7:1–5.

Rodríguez-Roda, J. (1983). Evolución de la pesquería del atún, *Thunnus thynnus* (L.), del golfo de Cádiz durante los años 1980 a 1982. *Investigación Pesquera*, 47(2):253–262.

Sarà, R. (1963). Données, observations et commentaires sur la présence, le comportement, les caractéristiques et les migrations des thons en Méditerranée. *Proceedings of the General Fisheries Council for the Mediterranean*, 7:371–388.

Sarà, R. (1980). Bluefin tuna trap fishery in the Mediterranean. *Collective Volume of Scientific Papers ICCAT*, 11:129–144.

Sinnott, R. (1984). Virtues of the haversine. *Sky and Telescope*, 68(2):159.

Smith, T., Reynolds, R., Peterson, T., and Lawrimore, J. (2008). Improvements to NOAA's Historical Merged Land-Ocean Surface Temperature Analysis (1880-2006). *Journal of Climate*, 21:2283–2296.

West, M. and Harrison, J. (1997). *Bayesian Forecasting and Dynamic Models*. Springer Verlag, New York, second edition.